Journal of Alloys and Compounds 509 (2011) 7186–7191

Contents lists available at ScienceDirect

Journal of Alloys and Compounds

journal homepage: www.elsevier.com/locate/jallcom

# Luminescence characteristics of $Lu_{0.8}Sc_{0.2}BO_3:RE^{3+}$ (RE = Eu, Tb) polycrystalline powders

Yuntao Wu, Dongzhou Ding, Shangke Pan, Fan Yang, Guohao Ren*

*Shanghai Institute of Ceramics, Chinese Academy of Sciences, No. 215 Chengbei Road, Jiading, Shanghai 201800, PR China*

ARTICLE INFO

*Article history:*
Received 6 December 2010
Received in revised form 7 April 2011
Accepted 9 April 2011
Available online 15 April 2011

*Keywords:*
Lutetium scandium orthoborate
Scintillation materials
Luminescence
Medical imaging
Thermoluminescence

ABSTRACT

$Lu_{0.8}Sc_{0.2}BO_3:RE^{3+}$ (RE = Eu, Tb) polycrystalline powders were prepared by high temperature solid state reaction method. The X-ray diffraction measurements confirmed that the doped materials were all monophasic solid solution powders. The influences of activator ion ($Eu^{3+}$ or $Tb^{3+}$) concentration on the photoluminescence and radioluminescence characteristics were investigated and discussed. The $Tb^{3+}$ doped materials showed excellent light yields than $Eu^{3+}$ doped materials under X-ray excitation. The fluorescence decay times of the optimal materials excited by UV were measured. Their defect properties were studied by thermoluminescence (TL) as a function of temperature (300–600 K) and the corresponding trap depth, frequency factor and detrapping time were theoretically calculated. The $Eu^{3+}$ and $Tb^{3+}$ ions were the unique recombination centers in corresponding samples. In addition, considering their attracting luminescence properties and excellent physical properties (high-density and non-hygroscope), the $Lu_{0.8}Sc_{0.2}BO_3:RE^{3+}$ (RE = Eu, Tb) can be used for X-ray medical imaging system, hence their crystal growth and characterizations deserve further investigation.



## 1. Introduction

Many applications such as high-energy physics, nuclear medical imaging and security inspection need inorganic scintillator materials composed of single crystals, usually doped with luminescence ion.

Due to the desired application, the performance of scintillation crystals should achieved by a compromise between characteristics (i.e. high density, high light output, fast response time) and chemical stability. Hence, many researchers are devoting to improving or optimizing the existing scintillation crystals [1–5], and also developing new scintillators such as $Y_2Si_2O_7$:Ce, $Gd_2Si_2O_7$:Ce, $Lu_2Si_2O_7$, $MgWO_4$ and so on [6–10]. Nevertheless, there are still many novel crystals deserved to be developed. The cerium activated lutetium orthoborate is one of the excellent promising scintillators [11–13]. In recent years, increased interest of researchers has been devoted to submicron and nanodimensional crystalline powders of cerium activated lutetium orthoborate, which is expected to be good prospect for the creation of effective scintillation films and composites [14–18].

However, because of the high-temperature phase transformation [19], it is very difficult to obtain $LuBO_3$ single crystal from its melt. Therefore, the growth of this crystal has always been regarded as an extremely difficult task. Nedelec et al. [20] once proposed that doping with rare earth ions can prevent the phase transformation in $LuBO_3$, but so far the specific rare earth ions that can stabilize the calcite phase or vaterite phase were not obtained. Recently, it was found that doping $Sc^{3+}$ can stabilize the calcite phase of $LuBO_3$ and the $Lu_{0.9}Sc_{0.1}BO_3:Ce^{3+}$ crystals were proposed for γ-ray applications [21,22]. In our earlier work [23], we reported the influence of Sc/Lu ratio on phase transformation and luminescence properties of $Lu_{1-x}Sc_xBO_3$:Ce solid solutions. Moreover, the $Lu_{0.8}Sc_{0.2}BO_3$:Ce crystal material has been obtained by Czochalski method and found to be a potential material for scintillation application [24]. Hence, in this work, we continue to explore the possibility of $Eu^{3+}$ or $Tb^{3+}$-doped materials to be efficient scintillators. The $Lu_{0.8}Sc_{0.2}BO_3:RE^{3+}$ (RE = Eu, Tb) materials were prepared by solid state method and studied luminescence properties as well as their thermoluminescence properties under ultraviolet light and X-ray excitation.

## 2. Experimental

Rare earth-doped lutetium scandium orthoborate solid solution polycrystals were synthesized in the muffle furnace by solid state reaction method. The starting materials are $Lu_2O_3$, $Sc_2O_3$, $B_2O_3$, $Eu_2O_3$ ($Tb_4O_7$) powder with 99.99% purity. They were weighed according to the stoichiometric ratio of $(Lu_{0.8}Sc_{0.2})_{1-x}RE_xBO_3$ (RE = Eu, Tb; $x$ = 0, 0.001, 0.003, 0.005, 0.01, 0.03) except for $B_2O_3$ which was 5 wt% rich due to vaporization loss during high-temperature synthesized, and then mixed for one hour, respectively. The pulverous mixtures were ground in an agate mortar and then reacted at 1500 °C for 15 h in Pt crucibles under CO reducing atmosphere for $Lu_{0.8}Sc_{0.2}BO_3:Tb^{3+}$ or air atmosphere for $Lu_{0.8}Sc_{0.2}BO_3:Eu^{3+}$, respectively. After these steps the temperature was slowly cooled down to room temperature.

* Corresponding author. Tel.: +86 21 69987740; fax: +86 21 59927184.
*E-mail address:* rgh@mail.sic.ac.cn (G. Ren).

0925-8388/$ – see front matter © 2011 Elsevier B.V. All rights reserved.
doi:10.1016/j.jallcom.2011.04.051

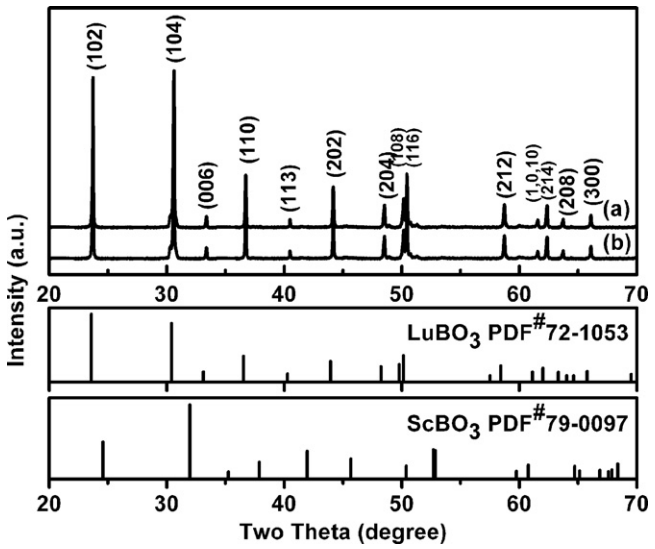


**Fig. 1.** X-ray diffraction patterns of $Lu_{0.8}Sc_{0.2}BO_3$:0.5 at%$Eu^{3+}$ (a) and $Lu_{0.8}Sc_{0.2}BO_3$:0.5 at%$Tb^{3+}$ (b) solid solutions with the corresponding PDF cards of $LuBO_3$ calcite phase and $ScBO_3$ calcite phase.

The phases of the obtained solid solutions were characterized by Rigaku D\max-2550 V (scanning rate = 2.4°/min at 40 kV and 50 mA) where Cu Kα was used as incident X-ray (XRD measurement).

The lattice parameters were calculated by the least-squares method using the JADE program (Materials Data Inc., Livermore, CA). The application of this method has been reported by other researchers [25,26]. The photoluminescence spectrum (PL and PLE) and fluorescence decay curves were recorded on the Perkin-Elmer LS50B and Jobin Yvon Fluorolog-3, respectively. The radioluminescence spectra were conducted on an X-ray Excited Luminescence Spectrometer, assembled at Shanghai Institute of Ceramics. The X-ray tube was operated at the condition of $V$ = 60 kV, $I$ = 2 mA. The powders were pressed into round tablets with smooth surface before measurements. The bismuth germinate (BGO) scintillation crystal was supplied by SICCAS and its absolute light yield was 8500 ph/MeV. The BGO crystal was fully grinded into powders to be used as reference. The thermoluminescence (TL) curves of crystal samples were determined with a FJ-427A1 thermoluminescence spectrometer with a linear heating rate of 1 K/s from 300 to 600 K. Prior to each TL measurement, the $Lu_{0.8}Sc_{0.2}BO_3$:0.3 at%$Tb^{3+}$ sample (~3 × 3 × 0.5 $mm^3$) and $Lu_{0.8}Sc_{0.2}BO_3$:0.5 at%$Eu^{3+}$ (~1 × 1 × 0.5 $mm^3$) were irradiated with X-ray for 90 s. Meanwhile, three-dimensional TL curves (the TL as a function of both the temperature and the wavelength, shorten as 3D TL) were also measured.

## 3. Results and discussion

### 3.1. XRD characterization

Fig. 1 presents the XRD patterns of $Lu_{0.8}Sc_{0.2}BO_3$:0.5 at%$RE^{3+}$ (RE = Eu, Tb) samples. In fact, whatever the doping ion and its concentration, the XRD patterns are nearly identical just with slight differences in diffraction angle. Hence, we present the representative patterns of $Lu_{0.8}Sc_{0.2}BO_3$:0.5 at%$RE^{3+}$ (RE = Eu, Tb) samples here. Both the experimental XRD patterns of these samples are identified by comparison with the calcite phase structure of lutetium orthoborate ($LuBO_3$, PDF#72-1053) and scandium orthoborate ($ScBO_3$, PDF#79-0079). It is found that the recorded diffraction patterns correspond exclusively to the calcite form of $LuBO_3$ with no evidence for $EuBO_3$ or $TbBO_3$ phases, just with slight diffraction angle difference. The calculated lattice constants of $Lu_{0.8}Sc_{0.2}BO_3$:0.5 at%$Eu^{3+}$ and $Lu_{0.8}Sc_{0.2}BO_3$:0.5 at%$Tb^{3+}$ are $a = b = 4.888$ Å $c = 16.086$ Å and $a = b = 4.893$ Å $c = 16.090$ Å, respectively, which are not completely satisfied with the Vegard-Law [27]. This is because the Vegard's law is just an approximation applicable to ideal solutions only when the difference in atomic radii or lattice parameters of the two components forming a solid solution is small (less than 5%) [28]. Herein, the difference in c lattice parameter of $LuBO_3$ and $ScBO_3$ is over 6% and the difference in atomic radius of Lu and Sc is over 7%. Consequently, it is reasonable to believe that the doped materials are all monophasic solid solution powders. It is also observed that the diffraction peaks of these samples are quite sharp and strong, indicating the final products are high crystallinity. As we know, the phosphors with high crystallinity have less traps and stronger luminescence.

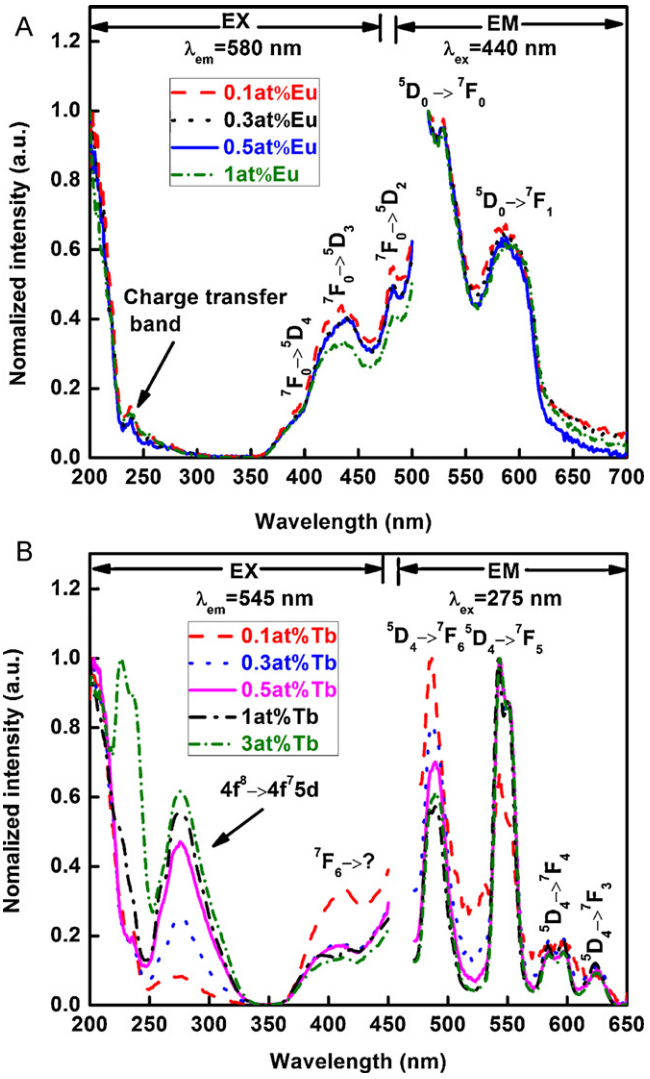


**Fig. 2.** Photoluminescence spectra of $Eu^{3+}$ (a) and $Tb^{3+}$ (b) doped $Lu_{0.8}Sc_{0.2}BO_3$ solid solution powders with different activator doping concentration recorded at room temperature.

### 3.2. PL and PLE properties of $Lu_{0.8}Sc_{0.2}BO_3$:$RE^{3+}$ (RE = Eu, Tb)

The PL and PLE spectra of $Lu_{0.8}Sc_{0.2}BO_3$:$RE^{3+}$ (RE= Eu, Tb) powders are measured at RT and is plotted in Fig. 2. The excitation spectra recorded for $Lu_{0.8}Sc_{0.2}BO_3$:$Eu^3$ powders all constitute of peaks corresponding to 4f–4f transitions. The peak at about 470 nm is attributed to $^7F_0 \rightarrow {}^5D_2$ transition and the ones situated in the range between 300 and 430 nm correspond to $^7F_0 \rightarrow {}^5D_4$, $^5D_3$ transitions respectively. The excitation band below 239 nm is assigned to the charge transfer absorption [29]. Meanwhile, the $^5D_0 \rightarrow {}^7F_0$ and $^5D_0 \rightarrow {}^7F_1$ are observed in the emission spectra, but the ratio of these two transitions is quite different from that of $LuBO_3$:1 at%$Eu^{3+}$ calcite form material [30].

For the $Lu_{0.8}Sc_{0.2}BO_3$:$Tb^{3+}$ samples, the typical 4f–4f emission, $^5D_4 \rightarrow {}^7F_6$, $^7F_5$, $^7F_4$, $^7F_3$ transitions [31], can be seen in the emission spectra. The $4f^8 \rightarrow 4f^7 5d$ transition peaking at 275 nm [32] and an

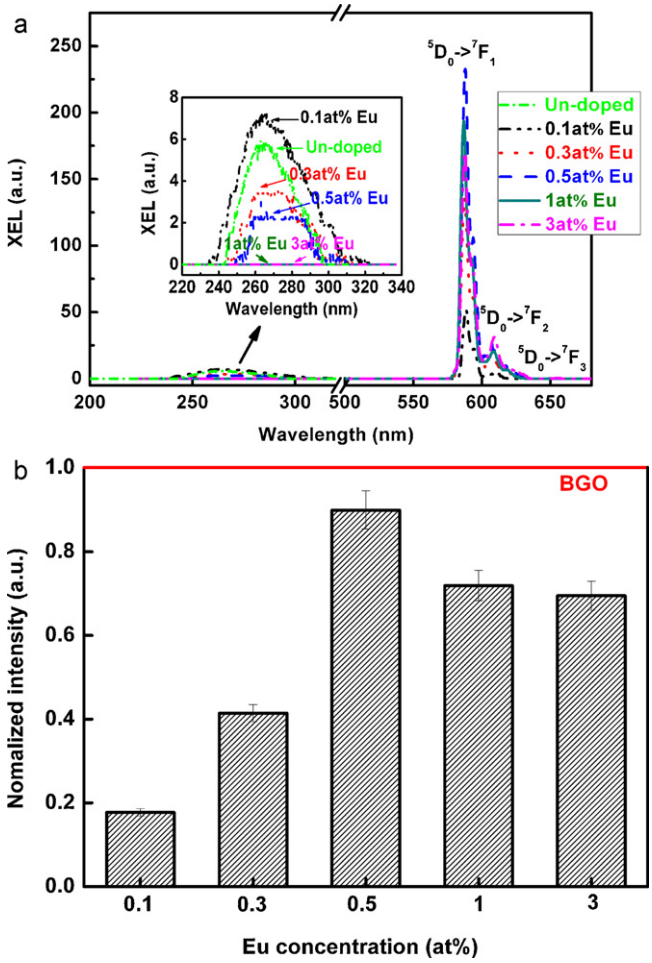


**Fig. 3.** XEL spectra of $Eu^{3+}$ doped $Lu_{0.8}Sc_{0.2}BO_3$ solid solution powders at room temperature (a) and normalized integrated intensity of $Lu_{0.8}Sc_{0.2}BO_3$:$Eu^{3+}$ comparing to BGO standard (b).

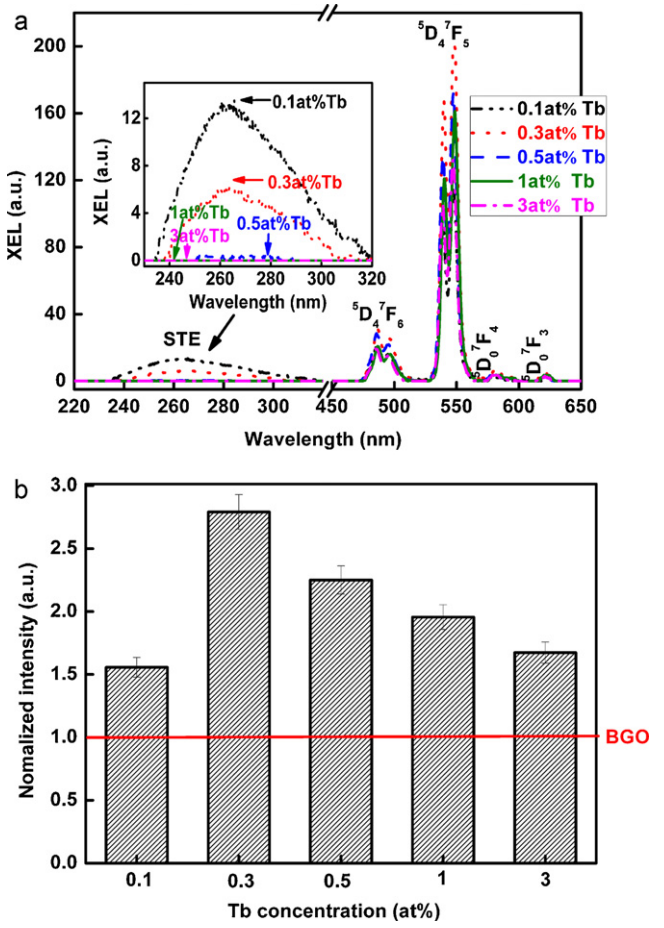


**Fig. 4.** XEL spectra of $Tb^{3+}$ doped $Lu_{0.8}Sc_{0.2}BO_3$ solid solution powders at room temperature (a) and normalized integrated intensity of $Lu_{0.8}Sc_{0.2}BO_3$:$Tb^{3+}$ comparing to BGO standard (b).

excitation band peaking at 405 nm can be observed in the excitation spectra. Moreover, since the excitation band peaking round 200 nm exists in both $Lu_{0.8}Sc_{0.2}BO_3$:$Eu^{3+}$ and the $Lu_{0.8}Sc_{0.2}BO_3$:$Tb^{3+}$ sample, we tentatively speculate that the origin of the band is host absorption not the transition belonging to activators, but it has not been fully resolved yet. In addition, it is worth to note that there is an abnormal increase between excitation and emission band for both the $Lu_{0.8}Sc_{0.2}BO_3$:$Eu^{3+}$ samples and the $Lu_{0.8}Sc_{0.2}BO_3$:$Tb^{3+}$ samples. We have adjusted the position of the sample and tried to minimize this effect, but the spectra still present the similar shapes. The influence of powder scattering and Sc-doping has been excluded, because this phenomenon has not been seen in the PL and PLE spectra of $Lu_{1-x}Sc_xBO_3$:$Ce^{3+}$ powder [23]. However, the cause of this phenomenon is still unknown. Although the part of the excitation and emission band can not be observed caused by the above phenomenon, the overall luminescence bands, such as host absorption, charge transfer, and the 4f–4f transitions, can be clearly determined.

### 3.3. *Radioluminescence properties of $Lu_{0.8}Sc_{0.2}BO_3$:$RE^{3+}$ (RE = Eu, Tb)*

The emission spectra recorded at room temperature under X-ray excitation for un-doped, $Eu^{3+}$ and $Tb^{3+}$ doped $Lu_{0.8}Sc_{0.2}BO_3$ are presented in Figs. 3 and 4. BGO emission spectrum has also been recorded in order to evaluate the luminescence intensity of $RE^{3+}$ doped materials. In Fig. 3a, the un-doped sample presents a self-trapped exciton (STE) emission band peaking at 260 nm [33]. For $Lu_{0.8}Sc_{0.2}BO_3$:$Eu^{3+}$ samples, beside a STE band, the spectrum is constituted of peaks corresponding to $^5D_0 \rightarrow {}^7F_J$ ($J$ = 0–3) transitions of $Eu^{3+}$ ions. The spectral distribution of the $Eu^{3+}$ doped materials results in a global orange–red emission. $Lu_{0.8}Sc_{0.2}BO_3$:$Tb^{3+}$ emission spectrum (Fig. 4a) shows, in the region from 475 to 650 nm, several lines characteristic of $^5D_4 \rightarrow {}^7F_J$ ($J$ = 3–6) transitions of $Tb^{3+}$ ions, and also a STE band. The most intensive transition is $^5D_4 \rightarrow {}^7F_5$, which results in an overall green emission. The results are well agreement with the previous report about the sol-gel derived $LuBO_3$:$Eu^{3+}$/$Tb^{3+}$ (Sc-free materials) [34], beside the existence of a STE band in our materials. It is also observed that the $^7F_0/^7F_1$ and $^7F_1/^7F_2$ ratios of $Eu^{3+}$-doped materials are changing upon X-ray excitation compared to PL spectra. We deduce that it is related to the different luminescence mechanism under different excitation source.

The X-ray excited light yields of $Lu_{0.8}Sc_{0.2}BO_3$:$RE^{3+}$ (RE = Eu, Tb) were determined by the ratio of the integrated intensity $I_{(LSBO:RE)}$ (the LSBO:RE is short for $Lu_{0.8}Sc_{0.2}BO_3$:$RE^{3+}$ (RE = Eu, Tb)) with that of the BGO reference sample, and then multiplied with the absolute light yield of BGO. Based on the integration of the $RE^{3+}$ emission bands in radioluminescence spectra, the yields can be calculated for the different samples and comparison with that of BGO standard. The equation is as follow:

$$N_{ph} = \frac{\int I_{LSBO:RE}(\lambda)\, d\lambda_{LSBO:RE}}{\int I_{BGO}(\lambda)\, d\lambda_{BGO}} \times 8500\ \text{photons/MeV} \quad (1)$$

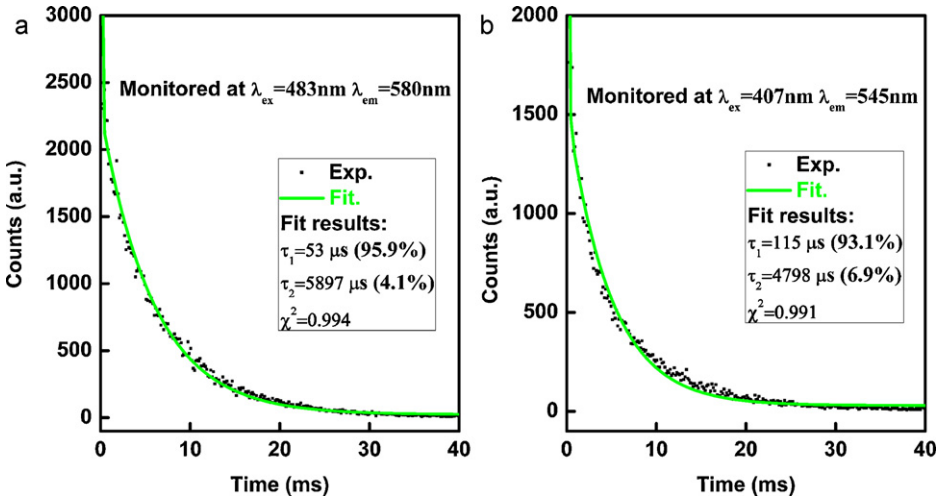


**Fig. 5.** Decay curves of $Lu_{0.8}Sc_{0.2}BO_3$:0.5 at%$Eu^{3+}$ (a) and $Lu_{0.8}Sc_{0.2}BO_3$:0.3 at%$Tb^{3+}$ (b) solid solutions recorded at room temperature.

By means of above mentioned equation, we can obtain the relative light yield of $Lu_{0.8}Sc_{0.2}BO_3$:$RE^{3+}$ (RE = Eu, Tb). According to the results shown in Fig. 3b, it can be seen that when the Eu ions doping concentration increases from 0.1 to 0.5 at%, the light yield of $Eu^{3+}$ increases considerably, and then decreases as the Eu concentration level increases further. The optimal light yield is achieved when the Eu doping concentration is 0.5 at% and the corresponding light yield is round 7700 ph/MeV. Fig. 4b shows that the optimal Tb ions doping concentration is 0.3 at% and the corresponding light yield could reach a good value 23,800 ph/MeV. For sol-gel derived $LuBO_3$:$Eu^{3+}$/$Tb^{3+}$ (Sc-free materials) [34], the optimal scintillation light yield are obtained for $Eu^{3+}$ and $Tb^{3+}$ content of 5 at% in both cases, namely 8923 ph/MeV and 4398 ph/MeV. By comparison, the light yield of Tb doped $LuBO_3$ has significantly improved by doping $Sc^{3+}$.

### 3.4. Fluorescence decay time and afterglow properties of $Lu_{0.8}Sc_{0.2}BO_3$:$RE^{3+}$ (RE = Eu, Tb)

The samples with optimal light yields, namely $Lu_{0.8}Sc_{0.2}BO_3$:0.5 at%$Eu^{3+}$ and $Lu_{0.8}Sc_{0.2}BO_3$:0.3 at%$Tb^{3+}$ solid solutions are chosen to measure fluorescence decay time. The fluorescence decay curves of $Lu_{0.8}Sc_{0.2}BO_3$:0.5 at%$Eu^{3+}$ and $Lu_{0.8}Sc_{0.2}BO_3$:0.3 at%$Tb^{3+}$ solid solutions under their most excitation wavelength at room temperature (RT) are shown in Fig. 5. The curves in Fig. 5 all can be well fitted by double exponential equation:

$$I = A_1 \exp\left(\frac{-t}{\tau_1}\right) + A_2 \exp\left(\frac{-t}{\tau_2}\right) + C \quad (2)$$

where $I_t$ and $I_0$ are luminescence intensities, $A$ is a constant, $t$ is the time, and $\tau_i$ ($i$ = 1, 2) are the decay time for the exponential components, respectively. The fitting decay time of $Eu^{3+}$ and $Tb^{3+}$ doped samples are found to be about 53 μs (95.9%), 5897 μs (4.1%), and 115 μs (93.1%), 4798 μs (6.9%), respectively. It is observed that there are slow components in both samples, but their proportions are quite small. Comparing with the typical X-ray excited luminescence materials, such as $Lu_2O_3$:Eu, LaOBr:Tb or $Gd_2O_2S$:Tb [35], the decay times of $Lu_{0.8}Sc_{0.2}BO_3$:0.5 at%$Eu^{3+}$ and $Lu_{0.8}Sc_{0.2}BO_3$:0.3 at%$Tb^{3+}$ samples are comparable and adequate for CT medical imaging system. In addition, the decay time of $Lu_{0.8}Sc_{0.2}BO_3$:0.3 at%$Tb^{3+}$ sample is apparently shorter than the value of $LuBO_3$:$Tb^{3+}$ (3.5 ms) reported by Yang [36]. Therefore, considering their attracting luminescence properties and excellent physical properties (high-density and non-hygroscope), the $Lu_{0.8}Sc_{0.2}BO_3$:$RE^{3+}$ (RE = Eu, Tb) can be used for X-ray medical imaging system, hence their crystal growth and characterizations deserve further investigation.

### 3.5. Thermoluminescence (TL) properties of $Lu_{0.8}Sc_{0.2}BO_3$:$RE^{3+}$ (RE = Eu, Tb)

TL is an effective method to study the trap characteristics of materials. We choose the samples with excellent luminescence properties to test their TL properties. The two-dimensional TL glow

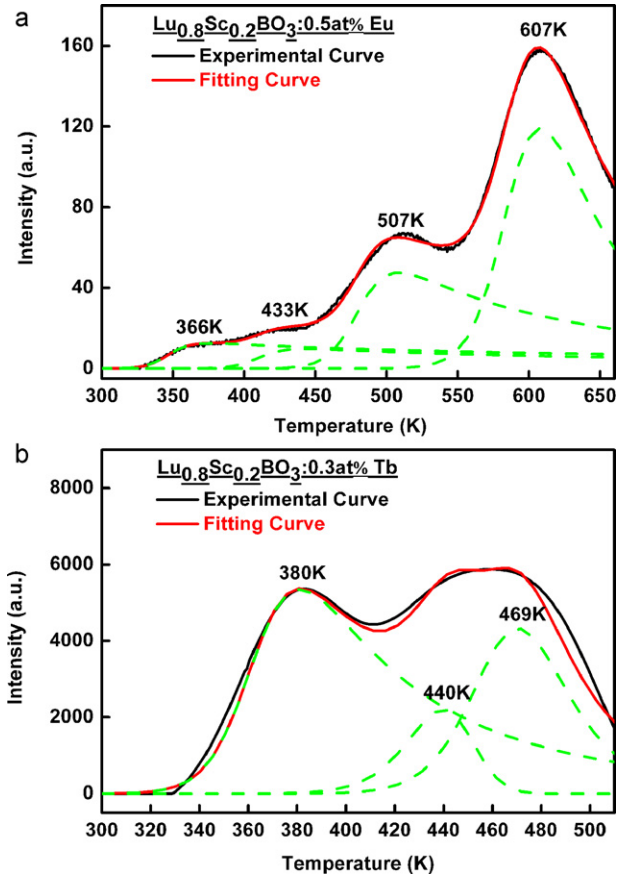


**Fig. 6.** 2D thermoluminescence spectra of $Lu_{0.8}Sc_{0.2}BO_3$:0.5 at%$Eu^{3+}$ (a) and $Lu_{0.8}Sc_{0.2}BO_3$:0.3 at%$Tb^{3+}$ (b) samples.

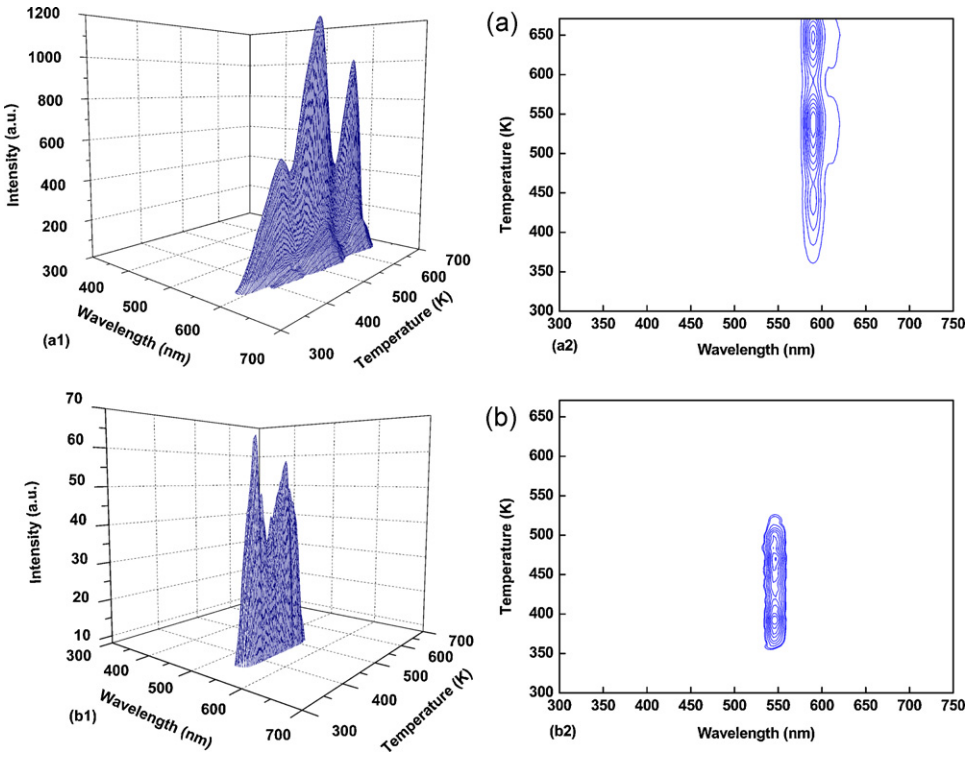


**Fig. 7.** 3D thermoluminescence spectra of $Lu_{0.8}Sc_{0.2}BO_3$:0.5 at%$Eu^{3+}$ (a) and $Lu_{0.8}Sc_{0.2}BO_3$:0.3 at%$Tb^{3+}$ (b) samples.

curves of $Lu_{0.8}Sc_{0.2}BO_3$:0.5 at%$Eu^{3+}$ and $Lu_{0.8}Sc_{0.2}BO_3$:0.3 at%$Tb^{3+}$ sample are shown in Fig. 6. The parameters of the charge traps corresponding to TL peaks can be obtained by analyzing the glow curves. Generally, the TL intensity $I$ as a function of temperature $T$ can be expressed as follow [37]

$$I(T) = sn_0 \exp\left(-\frac{E_t}{\kappa_B T}\right) \times \left[\frac{(l-1)s}{\beta}\int_{T_0}^{T} \exp\left(-\frac{E_t}{\kappa_B T}\right) dT + 1\right]^{-l/(l-1)} \quad (3)$$

Eq. (3) is a general form of the TL intensity $I$, as a function of temperature $T$. In the above equation, $n_0$ is the concentration of trapped charges at $t = 0$, $E_t$ is the energy level of the trap, $\kappa_B$ is the Boltzmann constant, $l$ is the kinetic order, $s$ is the frequency factor, and $\beta$ is the heating rate, 1 $Ks^{-1}$ in this measurement. Because Eq. (3) cannot be directly used to fit the experimental data, Eq. (4) developed by Feng [38] is adapted in the fitting process,

$$I(T) = sn_0 \exp\left(-\frac{E_t}{\kappa_B T}\right) \times \left\{\frac{(l-1)s}{\beta} \times T \times \exp\left(-\frac{E_t}{\kappa_B T}\right) \times \left[\left(\frac{\kappa_B T}{E_t}\right) - 2\left(\frac{\kappa_B T}{E_t}\right)^2 + 6\left(\frac{\kappa_B T}{E_t}\right)^3\right] + 1\right\}^{l/(1-l)} \quad (4)$$

The meanings of parameters are accordance with those in Eq (3). All the TL experimental data are fitted by using ORIGIN 8 software.

For the TL curve of Eu-doped sample, the single TL peak fitting result corresponds to the measured curve in the range of 450–550 K and 550–650 K, but not satisfying for the curve in the range of 300–450 K. It is implied that the actual curve between 300 and 450 K is formed by the overlap of two individual TL peaks. Moreover, it is found that the general kinetic order is the optimum fitting model for all the TL peaks. The TL curve of Tb-doped sample can be fitted in the same way in the range of 300–500 K. A good agreement between the experimental data and the simulated data is obtained and also shown in Fig. 6, and the calculated TL parameters are listed in Table 1. According to the fitting results, the TL glow curve of Eu-doped sample consists of a dominant band peaking at 607 K and three relatively weak peaks at 366, 433 and 507 K. While, Tb-doped sample have three TSL peaks, namely 380, 440, and 469 K. While the detrapping time at any temperature T can be can calculated as

$$\tau = s^{-1} \exp\left(\frac{E}{kT}\right) \quad (5)$$

where $E$ (eV) is the temperature of the peak, $k$ is the Boltzmann constant. Trap depth, frequency factor, and detrapping time at $RT$ are reported in Table 1 for all the TL peaks. The 3D TL of Eu-doped and Tb-doped samples, shown in Fig. 7, show a typical $Eu^{3+}$ 4f–4f transition and $Tb^{3+}$ 4f–4f transition, respectively. It suggests that the $Eu^{3+}$ and $Tb^{3+}$ ions are the unique recombination luminescence centers

**Table 1**
Parameters of TL glow curve peaks corresponding to $Lu_{0.8}Sc_{0.2}BO_3$:0.5 at%$Eu^{3+}$ and $Lu_{0.8}Sc_{0.2}BO_3$:0.3 at%$Tb^{3+}$ samples.

| | Peak temperature (K) | $E$ (eV) | $n_0$ | $s$ ($s^{-1}$) | $\tau$ (s) |
|---|---|---|---|---|---|
| $Lu_{0.8}Sc_{0.2}BO_3$:0.5 at%$Eu^{3+}$ | 366 | 1.35 | $3.32 \times 10^4$ | $1.56 \times 10^{16}$ | 60 |
| | 433 | 1.55 | $5.62 \times 10^3$ | $2.07 \times 10^{16}$ | 51 |
| | 507 | 1.80 | $7.28 \times 10^3$ | $5.01 \times 10^{16}$ | 15 |
| | 607 | 2.15 | $7.30 \times 10^3$ | $6.48 \times 10^{16}$ | 11 |
| $Lu_{0\text{-}8}Sc_{0.2}BO_3$:0.3 at%$Tb^{3+}$ | 380 | 1.14 | $4.77 \times 10^5$ | $8.39 \times 10^{13}$ | 16 |
| | 440 | 1.36 | $6.73 \times 10^4$ | $3.57 \times 10^{14}$ | 10 |
| | 469 | 1.48 | $1.84 \times 10^5$ | $7.05 \times 10^{14}$ | 11 |

for the detrapped charge carriers, respectively. It is observed that the detrapping times at RT calculated for all the TSL peaks of Eu- and Tb-doped samples are longer than 10 s, we tentatively speculate that the mediated recombination mechanism is accomplished by thermally induced electron detrapping into conduction band followed by the delayed electron–hole recombination at activator center. The above process will undoubtedly result in the luminescence loss. However, as we know, the luminescence loss is more directly associated with the shallow traps rather than the deep ones [39]. According to the results of Eu- and Tb-doped samples (shown in Figs. 3b and 4b), it is believed that the Eu-doped sample must have shallower traps in the band gap than Tb-doped sample. Due to the equipment constrain, we could not supply related low-temperature (25–275 K) TL data here, but the corresponding work is undergoing.

## 4. Conclusions

$Lu_{0.8}Sc_{0.2}BO_3:RE^{3+}$ (RE = Eu, Tb) were prepared by high temperature solid state reaction method. The doped materials were all monophasic solid solution powders. The influences of activator ion ($Eu^{3+}$ or $Tb^{3+}$) concentration on the photoluminescence characteristics were investigated and discussed. The $Tb^{3+}$ doped materials showed excellent light yields than $Eu^{3+}$ doped materials under X-ray excitation. The fluorescence lifetimes of the optimal materials were 53 μs for $Lu_{0.8}Sc_{0.2}BO_3$:0.5 at%$Eu^{3+}$ and 115 μs for $Lu_{0.8}Sc_{0.2}BO_3$:0.3 at%$Tb^{3+}$ respectively. Their defect properties were studied by thermoluminescence (TL) as a function of temperature (300–600 K) and the corresponding trap depth and frequency factor were calculated theoretically. The $Eu^{3+}$ and $Tb^{3+}$ ions were the unique recombination centers in corresponding samples. In addition, considering their attracting luminescence properties and excellent physical properties (high-density and non-hygroscope), the $Lu_{0.8}Sc_{0.2}BO_3:RE^{3+}$ (RE = Eu, Tb) can be used for X-ray medical imaging system, hence their crystal growth and characterizations deserve further investigation.

## Acknowledgements

We thank Prof. Martin Nikl of Institute of Physics, Academy of Science Czech Republic for useful discussions on the subject of this paper. This work was supported by the National Natural Science Foundation of China (Grant No. 50902145), the Natural Science Foundation of Shanghai (Grant No. 09ZR1435800), and the Knowledge Innovation Program of the Chinese Academy of Sciences (Grant No. SCX200701).

## References

[1] G.H. Ren, X.F. Chen, Y. Pei, H.Y. Li, H.X. Xu, J. Alloys Compd. 467 (2009) 120–123.
[2] P.S. Yu, A.H. Wu, L.B. Su, X. Guo, Y.B. Wang, H.Y. Zhao, Y. Yang, Q.H. Yang, J. Xu, J. Alloys Compd. 503 (2010) 380–383.
[3] D.H. Cao, G.J. Zhao, J.Y. Chen, Q. Dong, Y.C. Ding, Y. Cheng, J. Alloys Compd. 489 (2010) 515–518.
[4] F. Yang, S.K. Pan, D.Z. Ding, X.F. Chen, S. Lu, W.D. Zhang, G.H. Ren, J. Alloys Compd. 484 (2009) 837–840.
[5] M. Gu, L.C. Jia, X.L. Liu, S.M. Huang, B. Liu, C. Ni, J. Alloys Compd. 502 (2010) 190–194.
[6] F.A. Danevich, D.M. Chernyak, A.M. Dubovik, B.V. Grinyov, S. Henry, H. Kraus, V.M. Kudovbenko, V.B. Mikhailik, L.L. Nagornaya, R.B. Podviyanuk, O.G. Polischuk, I.A. Tupitsyna, Yu. Ya. Vostretsov, Nucl. Instrum. Methods Phys. Res. A 608 (2009) 107–115.
[7] H. Feng, D.Z. Ding, H.Y. Li, S. Lu, S.K. Pan, X.F. Chen, G.H. Ren, J. Alloys Compd. 489 (2010) 645–649.
[8] H. Feng, D.Z. Ding, H.Y. Li, S. Lu, S.K. Pan, X.F. Chen, G.H. Ren, J. Alloys Compd. 509 (2011) 3855–3858.
[9] O. Sidletskiy, V. Baumer, I. Gerasymov, B. Grinyov, K. Katrunov, N. Starzhinsky, O. Tarasenko, V. Tarasov, S. Tkachenko, O. Voloshina, O. Zelenskaya, Radiat. Meas. 45 (2010) 365–368.
[10] A. Zych, A.L. op Reinink, K. van der Eerden, C. de Mello Donegá, A. Meijerink, J. Alloys Compd. 509 (2011) 4445–4451.
[11] M.J. Weber, S.E. Derenzo, C. Dujardin, W.W. Moses, Proceedings of the International Conference on Inorganic Scintillators and Their Applications, September, 1995, pp. 325–328.
[12] W.W. Moses, M.J. Weber, S.E. Derenzo, D. Perry, P. Berdahl, Proceedings of the International Conference on Inorganic Scintillators and Their Applications, September, 1997, pp. 22–25.
[13] L. Zhang, C. Pedrini, C. Madej, C. Dujardin, J.C. Ga^con, B. Moine, I. Kamenskikh, A. Belsky, D.A. Shaw, M.A. MacDonald, P. Mesnard, C. Fouassier, J.C. Van't Spijker, C.E.W. Van Eijk, Radiat. Eff. Defects Solids 150 (1–4) (1999) 47–52.
[14] D. Boyer, F. Leroux, G. Bertrand, R. Mahiou, J. Non-Cryst. Solids 306 (2002) 110–119.
[15] C. Mansuy, E. Tomasell, R. Mahiou, L. Gengembre, J. Grimblot, J.M. Nedelec, Thin Solid Films 515 (2006) 666–669.
[16] C. Mansuy, J.M. Nedelec, R. Mahiou, J. Mater. Chem. 14 (2004) 3274–3280.
[17] J. Yang, C.X. Li, X.M. Zhang, Z.W. Quan, C.M. Zhang, H.Y. Li, J. Lin, Chem. Eur. J. 14 (2008) 4336–4345.
[18] C. Mansuy, J.M. Nedelec, C. Dujardin, R. Mahiou, J. Sol–Gel Sci. Technol. 32 (2004) 253–258.
[19] E. Levin, R.S. Roth, J.B. Martin, Am. Mineral. 46 (1961) 1030–1055.
[20] J.-M. Nedelec, L. Courtheoux, E. Jallot, C. Kinowski, J. Lao, P. Laquerriere, C. Mansuy, G. Renaudin, S. Turrell, J. Sol–Gel Sci. Technol. 46 (2008) 259–271.
[21] S. Hatamoto, T. Yamazaki, J. Hasegawa, M. Katsurayam, M. Oshika, Y. Anzai, J. Cryst. Growth 311 (2009) 530–533.
[22] T. Yanagida, Y. Fujimoto, N. Kawaguchi, Y. Yokota, K. Kamada, D. Totsuka, S. Hatamoto, A. Yoshikawa, V. Chani, Nucl. Instrum. Methods Phys. Res. A (2010), doi:10.1016/j.nima.2010.08.115.
[23] Y.T. Wu, D.Z. Ding, S.K. Pan, F. Yang, G.H. Ren, J. Alloys Compd. 509 (2011) 366–371.
[24] Y.T. Wu, D.Z. Ding, S.K. Pan, F. Yang, G.H. Ren, Cryst. Res. Technol. 46 (2011) 48–52.
[25] Y. Harada, D.C. Dunand, Mater. Sci. Eng. A 329–331 (2002) 686–695.
[26] L.Y. Li, D.M. Strachan, H. Li, L.L. Davis, M.X. Qian, J. Non-Cryst. Solids 272 (2000) 46–56.
[27] A.R. Denton, N.W. Ashcroft, Phys. Rev. A 43 (1991) 3161–3164.
[28] K.T. Jacob, L. Shubhra Raj, Rannesh, Int. J. Mater. Res. 9 (2007) 776–779.
[29] D. Hreniak, E. Zych, L. Kepinski, W. Strek, J. Phys. Chem. Solids 64 (2003) 111–119.
[30] D. Boyer, G. Bertrand-Chadeyron, R. Mahiou, L. Lou, A. Brioude, J. Mugnier, Opt. Mater. 16 (2001) 21–27.
[31] M. Zawadzki, D. Hreniak, J. Wrzyszcz, W. Mista, H. Grabowska, O.L. Malta, W. Strek, Chem. Phys. 291 (2003) 275–285.
[32] L.H. Tian, S.I. Mho, B.Y. Yu, H.L. Park, J. Korean Phys. Soc. 47 (2005) 1070–1073.
[33] S.P. Feofilov, Y. Zhou, J.Y. Jeong, D.A. Keszler, R.S. Meltzer, J. Lumin. 125 (2007) 80–84.
[34] C. Mansuy, J.M. Nedelec, C. Dujardin, R. Mahiou, Opt. Mater. 29 (2007) 697–702.
[35] M. Nikl, Meas. Sci. Technol. 17 (2006) 37–54.
[36] J. Yang, C.M. Zhang, L.L. Wang, Z.Y. Hou, S.S. Huang, H.Z. Lian, J. Lin, J. Solid State Chem. 181 (2008) 2672–2680.
[37] D.W. Cooke, B.L. Bennett, E.H. Farnum, W.L. Hults, Appl. Phys. Lett. 70 (1997) 3594–3596.
[38] H. Feng, D.Z. Ding, H.Y. Li, S. Lu, S.K. Pan, X.F. Chen, G.H. Ren, J. Appl. Phys. 103 (2008), 083109-1-083109-7.
[39] M. Nikl, E. Mihokova, J. Pejchal, A. Vedda, M. Fasoli, I. Fontana, V.V. Laguta, V. Babin, K. Nejezchleb, A. Yoshikawa, H. Ogino, G. Ren, IEEE Trans. Nucl. Sci. 55 (2008) 1035–1041.